Unraveling Ligand Exchange Reactions in Linear Neutral Au(I) and Cu(I) N-heterocyclic carbene complexes for Biological Applications.

*Gustavo C. Rodrigues, Manoel V. F. Barrionuevo, Miguel A. San-Miguel, Camilla Abbehausen**

Institute of Chemistry, University of Campinas – UNICAMP, P.O. Box 6154, CEP 13083-970, Campinas, São Paulo, Brazil.

*Corresponding author: camilla@unicamp.br

KEYWORDS

Gold, copper, N-heterocyclic carbenes, metallodrugs, DFT

ABSTRACT

This study employed semiempirical GFN-xTB and density functional theory (DFT) calculations to investigate ligand exchange reactions of linear complexes [M(NHC)Cl] (M = Au(I) or Cu(I), NHC = N-heterocyclic carbenes) relevant to medicinal chemistry. Despite their potent in vitro antitumor, antibacterial, and antiparasitic activities, speciation limits their application. The research explored three biologically relevant reactions. Firstly, chloride substitution with dimethylsulfoxide (DMSO), the solvent used to prepare stock solutions before in vitro studies. Secondly, ligand scrambling involves the rearrangement of ligands in solution forming $[M(NHC)_2][MCl_2]$. Lastly, chloride substitution with cysteine, a biologically relevant ionic amino acid. Thermodynamically and kinetically, chloride replacement by DMSO is less favorable than ligand scrambling, particularly for Cu(I) complexes, suggesting [M(NHC)Cl] is the most abundant species present followed by $[M(NHC)_2][MCl_2]$, the last mainly in Cu(I) complexes. Cysteine substitution proves to be the most thermodynamically and kinetically favorable, potentially impacting the biological mechanism of action. The study also compares reaction mechanisms between Au(I) and Cu(I) complexes by analyzing transition state geometries. This research enhances understanding of ligand exchange reactions in linear complexes, shedding light on thermodynamic and kinetic preferences and biological mechanisms. The insights from the current work aid the interpretation of *in vitro* and *in vivo* data, unlocking the potential of these complexes for medicinal applications.

INTRODUCTION

Group 11 coinage metals, copper, silver, and gold, contribute to the pool of elements in the design of metal-based drugs. Although they belong to the same family, their chemistry is diverse, resulting in several biological outcomes.

Gold(I) compounds have been employed in medicine since ancient times, primarily for treating tuberculosis[1]. Then, gold thiolates, including aurothiomalate, aurothioglucose, and auranofin, are FDA-approved drugs for treating rheumatoid arthritis and other autoimmune conditions[2]. The potent anti-inflammatory response of Au(I) compounds stimulated their investigation for various disease treatments, such as cancer[3], bacterial[4], parasitic[5], and viral infections[6,7].

On the other hand, copper complexes have shown potential as drugs for several diseases, but mostly the research is limited to academia[8]. The growing interest in copper-based drugs is driven by the fact that copper is an essential element for humans, and cells have the machinery to regulate its absorption and excretion, thereby improving pharmacodynamics[9–11].

Gold(I) and Cu(I) compounds typically have a coordination number of two and a linear geometry; therefore, higher coordination numbers and different geometries, such as trigonal and tetrahedral, have been reported[12]. These compounds can also form polymers, as in aurothioglucose, aurothiomalate, Cu(I)-thiobenzamide, and Cu(I)-piperazine[13,14]. Additionally, both Au(I) and Cu(I) can establish M-M interactions, which occur in a range of Au(I) and Cu(I)-containing molecules, from di- to supramolecular structures[15,16].

Various ligands, including phosphines, organometallic carbenes, and alkynyl, can stabilize Au(I) or Cu(I) molecules, preventing polymerization, reduction, and slowing ligand substitution

reactions[17]. Among these, N-heterocyclic carbenes (NHCs) are particularly notable due to their strong σ-donation and π-reception ability, and the facility to tune their electronic and steric properties, allowing for metal complexes design with specific characteristics. Cationic $[M(NHC)_2]^+$ and neutral [M(NHC)Cl] complexes have been explored as drug chemotypes for anticancer, antibacterial, antiparasitic, and antiviral agents[6,8,18–20]. These soft Pearson's acids bind to cysteine or selenocysteine through a ligand exchange reaction with essential enzymes, such as thioredoxin[21], trypanothione[22], glutathione reductases[23], cysteine protease[20], and Cys-rich proteins such as zinc-fingers. However, their unselective binding to biomolecules limits their application *in vivo*, despite their excellent results *in vitro*[24].

To address this issue, ligand substitution reactions for linear M(I) complexes with several ligands have been studied experimentally and theoretically[6,8,25,26]. In general, complexes [M(I)LX], where L can be a phosphine or carbene, X any halide, and M a group 11 element, can be attacked by nucleophiles (:B), including solvent molecules, exchanging the halide, resulting in $[MLB]^{n+}$. However, [MLX] complexes can also undergo ligand scrambling when two molecules interact, generating $[ML_2]^+$ $[MX_2]^-$ in solution[27]. In the case of Au(I)-NHC, mechanistic studies are focused on ligand replacement reactions between cationic $[M(NHC)_2]^+$ and cysteine or selenocysteine[28–30]. For neutral [M(NHC)X], studies are focused on the ligand scrambling mechanism[31]. Our research group has studied the leishmanicidal and antiviral activity of several Au(I) and Cu(I)-NHC complexes, with promising results[6,8]. Among the compounds, [Au(I)(IMes)Cl] and [Cu(I)(IMes)Cl], where IMes is [1,3-bis(2,4,6-trimethylphenyl)-2H-imidazol-2-ylidene], were the most promising. ^{1}H NMR and ESI-MS studies in dimethyl sulfoxide (DMSO), DMSO/H_2O, and acetonitrile (CH_3CN) showed that solvent substitution and ligand scrambling reactions were significant for [Cu(I)(IMes)Cl], while for [Au(I)(IMes)Cl], these reactions were less prominent[6,8].

According to our studies, the ligand scrambling depends on the steric hindrance of R groups in NHC and solvent permittivity[8]. The *in vitro* investigation of these compounds in cell culture is usually performed in DMSO/aqueous medium. Thus, this study considers the solvent replacement of chlorides as one of the possible reactions of these compounds in DMSO solution, in addition to the ligand scrambling (Scheme 1).

Moreover, we investigated their replacement with cysteine in the thiolate form (Cys^-) to explain the reaction observed experimentally in our previous studies, including the inhibition of cysteine protease[20]. The results provide a deeper insight into the active species present in the *in vitro* testing, allowing a better understanding of biological outcomes and structure-activity relationships.

Scheme 1. Representation of the reaction routes studied. (I) Reaction with DMSO, (II) Reaction with Cys^-, (III) ligand scrambling reaction.

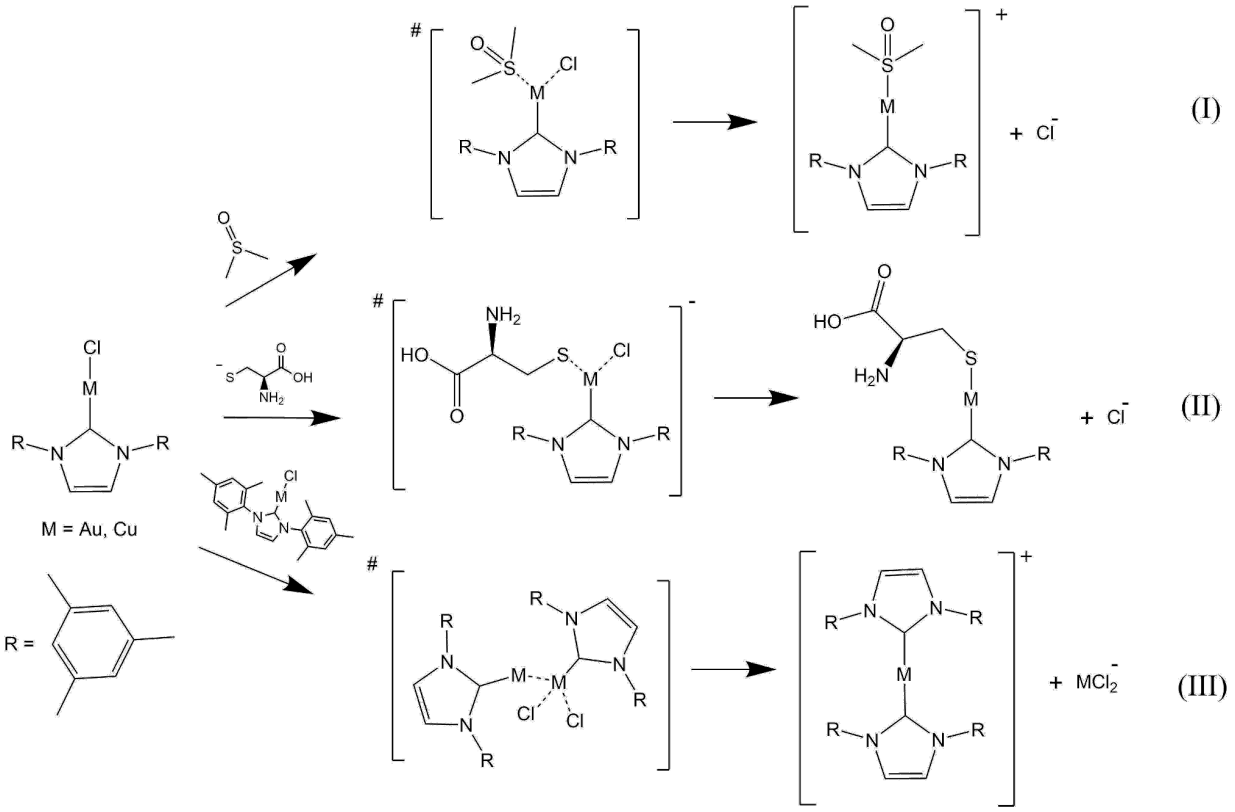

COMPUTATIONAL DETAILS

Initially, the structures of the reactants, DMSO, Cys^- (the *L* ligands), [Au(IMes)Cl], [Cu(IMes)Cl], and the products of these reactions, [Au(IMes)*L*], [Cu(IMes)*L*], $[Au(IMes)_2]^+$, $[Cu(IMes)_2]^+$, $[AuCl_2]^-$, $[CuCl_2]^-$ and Cl^- were optimized by DFT, using ORCA package version 5.0.1[32,33]. The functional PBE0[34], def2-TZVP/BJ basis functions[35], RIJCOSX approximation[36], and CPCM for implicit DMSO solvation were applied for all molecules[37]. ZORA relativistic correction was used for Au(I)-based compounds[38]. Frequency calculations were performed at the same level of theory to verify the minimum structures. From the optimized geometries, the Fukui functions f^+ and f^- for the complexes [Au(IMes)Cl], [Cu(IMes)Cl], and ligands *L* were also calculated,

defining the initial reaction coordinates[39,40]. In addition to the structures of separate reagents and products, optimization calculations of the reagents adducts (RA) and product adducts (PA) of the studied reactions were carried out using the same level of theory. The relaxed surface scanning method was used to search for candidate transition state (TS) structures. From the optimized TS geometries, scans were performed for each reaction coordinate defined by Fukui function surfaces, seeking to bring the most nucleophilic atoms of *L* closer to the most electrophilic center of the complex. The scans for the DMSO and ligand scrambling reactions were performed using the third level of the semi-empirical quantum mechanical method GFN-xTB, with an accuracy of 0.0001 hartree (Eh) in 120 steps[41]. In the case of Cys^- reactions, scans were carried out in 15 steps using DFT, employing the PBE0 functional, def2-TZVP/BJ basis functions, RIJCOSX approximation, ZORA relativistic correction, and CPCM for implicit DMSO solvation, that is, the same level of theory previously used in the optimization of reagents and products structures.

Then, all structures were manually screened to choose 5 to 10 candidates TS, for the DMSO and ligand scrambling scans, and 3 for the Cys^- scans, which were subjected to a subsequent optimization step by DFT following the lowest energy eigenvalues respective to the reaction coordinates of interest. TS optimization employed the same level of theory previously used in the reagents and product optimization. The parameters of the manual screening were chosen based on what is known about the transition state theory, i.e., their energies should comprise a maximum in the reaction coordinate presenting only one negative vibrational normal mode that relates to the reaction coordinate of the studied process.

Once the TS optimizations were completed, the corrected energies of all reaction participants were calculated to obtain graphs of levels of variation in free energy, including the calculated energies of reactant adducts (RA) and products adducts (PA). These illustrate the variation of

Gibbs free energy (ΔG), by the energy difference between products and reagents and activation energy (Ea), by the difference between the energies of reagents and the optimized TS.

RESULTS

The optimized R, P, RA, and PA geometries from the six studied reactions were confirmed to be at a local minimum by frequency calculations. Structural parameters, such as bond length and angles, of the optimized [Au(IMes)Cl] and [Cu(IMes)Cl] structures (Figures 1 and S1, respectively) are in agreement with those of experimental crystal structures of the molecules (Table S1)[42,43].

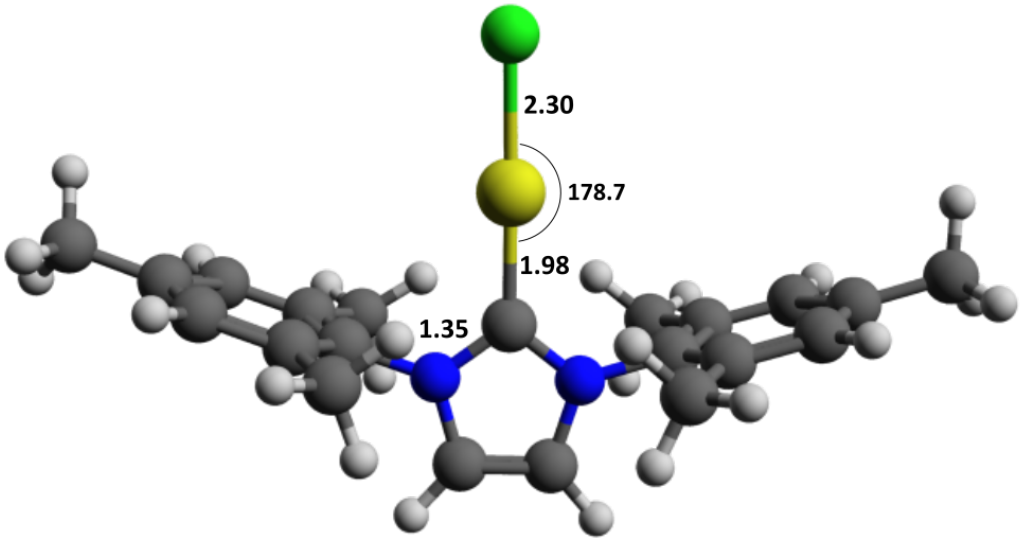

Figure 1. Optimized structures of [Au(IMes)Cl]. The main distances (Å) and angles (degrees) are indicated. Black, grey, blue, yellow, and green spheres depict carbon, hydrogen, nitrogen, gold, and chlorine atoms.

Although the amino acid cysteine has a thiol group with pKa 8.3, in most of the active sites of drug targets such as glutathione reductase, trypanothione reductase, and cysteine protease, Cys

neighbors a His that activates Cys by deprotonation of the thiol group[44]; therefore, in this work, Cys^-, in thiolate form, was considered in the reactions.

The calculated Fukui f^+ surfaces for the DMSO and Cys^- molecules (Figure S2) qualitatively indicate that sulfur is the most nucleophilic atom in both molecules. Moreover, the f^- Fukui surface of the [Au(IMes)Cl] and [Cu(IMes)Cl] complexes (Figure S3) showed a region of maximum around the Au(I) and Cu(I) cations, respectively, indicating the most electrophilic center of the molecule. These results were then used to define the reaction coordinates for the substitution reactions. The f^+ surfaces of [Au(IMes)Cl] and [Cu(IMes)Cl] exhibited maximum values around the nitrogen and carbon atoms in the IMes ligand. Therefore, the coordinate for the ligand scrambling reaction was defined as the proximity of the carbon atom in one of the [M(IMes)Cl] molecules to the M(I) center of the other molecule.

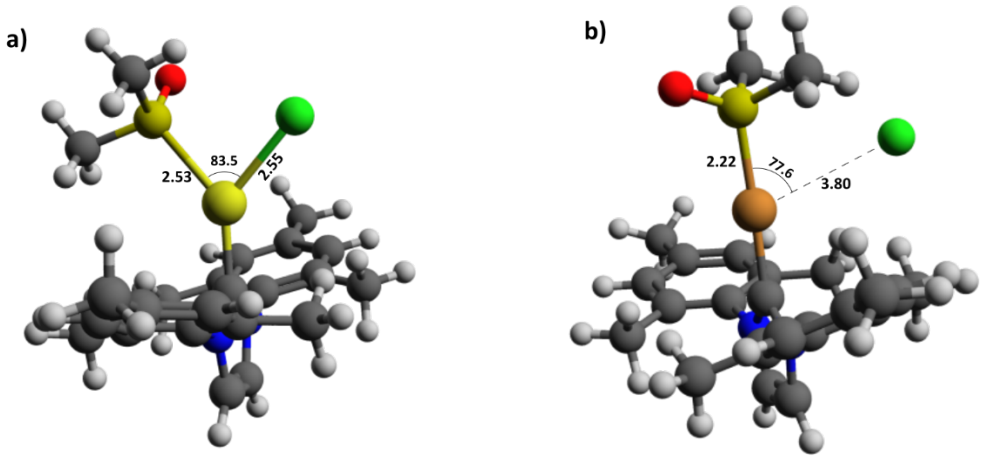

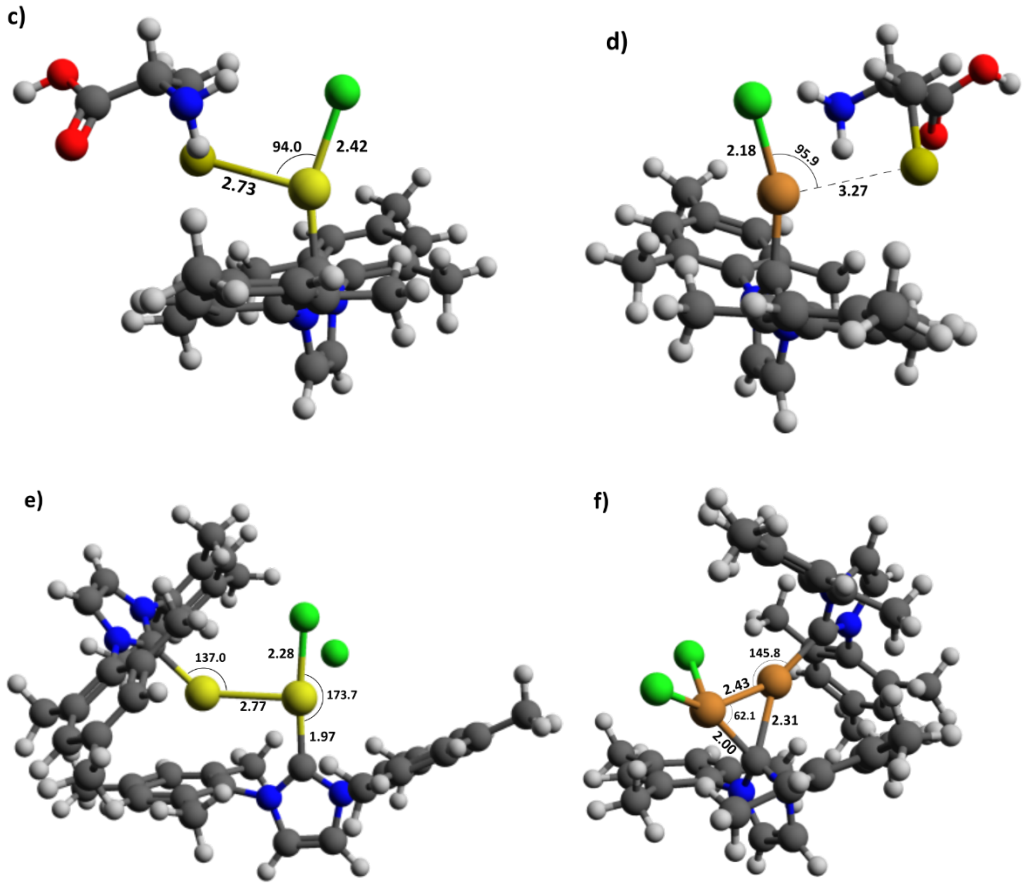

Figure 2. Structures of transition states for the reaction of [Au(IMes)Cl] and [Cu(IMes)Cl] with (a) and (d) DMSO, (b) and (e) Cys^- and (c) and (f) scrambling, respectively.

Regarding the TS optimization, at least one converged structure was obtained for all reactions, which presents the formation of a metal and *L* bond and a subsequent leaving of the Cl^- halide, evidence of coherent transition states (Figure 3). However, the optimization of TS candidates obtained for the Cys^- reactions, for both [Au(IMes)Cl] and [Cu(IMes)Cl], using GFN-xTB yielded TS structures that did not exhibit any negative vibrational modes associated with the reaction coordinate of interest. As such, a more refined approach involving a higher level of theory was employed for the Cys^- reaction as an alternative, ultimately producing coherent TS structures.

The Gibbs free energy and enthalpy variations for the reaction steps are reported in Table 1. Figures 3a-c illustrate the energy variation as a function of the coordinate for each reaction.

Table 1. Enthalpies and Gibbs free energy for the steps of the reactions (kJ/mol).

Reaction	**R → P**		**R → TS**		**R → RA**		**RA → PA**	
[Au(IMes)Cl]	ΔH	ΔG	ΔH	ΔG	ΔH	ΔG	ΔH	ΔG
DMSO	50.24	77.59	47.07	101.42	-1.99	55.95	41.23	41.83
Cys^-	-67.20	-32.67	6.71	69.70	-1.51	55.80	-67.08	-69.77
Scrambling	22.59	58.70	124.55	196.15	-2.18	58.07	19.30	31.29
[Cu(IMes)Cl]	ΔH	ΔG	ΔH	ΔG	ΔH	ΔG	ΔH	ΔG
DMSO	57.34	84.55	35.16	103.83	-6.99	53.34	54.23	46.68
Cys^-	-38.43	-13.62	-314.68	55.89	-1.72	52.58	-45.87	-37.26
Scrambling	7.16	49.80	47.34	128.09	-2.80	60.28	1.60	16.93

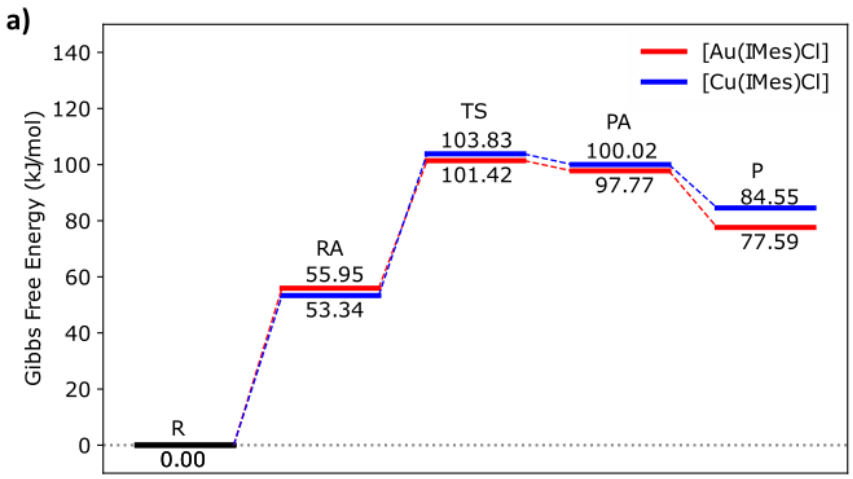

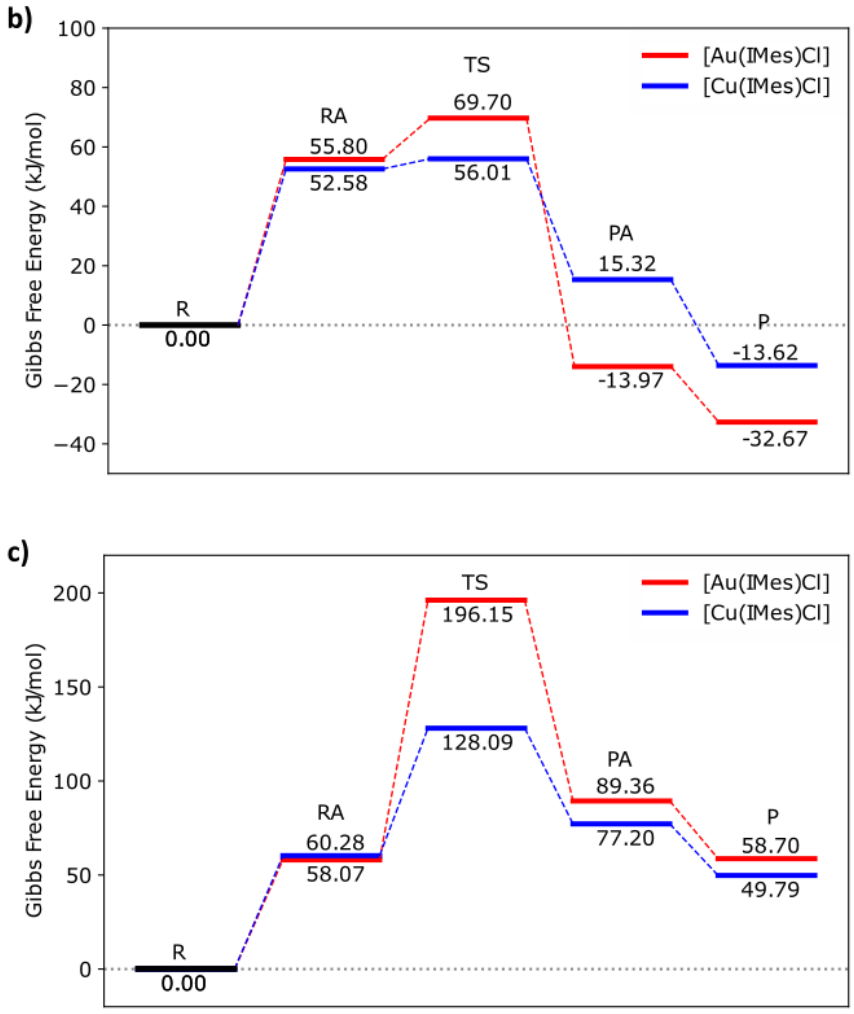

Figure 3. Reaction profiles of the three ligand replacement of [Au(IMes)Cl] and [Cu(IMes)Cl] with the following reagents a) DMSO b) Cys^- and c) ligand scrambling

DISCUSSION

The energies (Figure 3a) show reactions with DMSO are highly endergonic, with similar reaction profiles for [Au(IMes)Cl] and [Cu(IMes)Cl], which might be due to charge separation after the reaction. The charge separation is evidenced by the variation in the Mulliken atomic charges of the relevant partially charged atoms during the reaction, with a greater variation observed for the metal atom in the DMSO substitution compared to the Cys^- reaction (Table S2).

Also, the barrier is considerably high (R→TS), around 100 kJ/mol (23.88 kcal/mol), suggesting the reaction is unfavorable for both complexes. In contrast, the reaction with Cys^- is exergonic for Au(I) and Cu(I) complexes, (RA→PA) -69.77 (-16.66 kcal/mol) and -37.26 kJ/mol (-8.89 kcal/mol).

Although the Au(I) and Cu(I) metal centers of the complexes are isoelectronic, the studied reactions of [Au(IMes)Cl] and [Cu(IMes)Cl] seem to occur via different mechanisms, as observed by the structural differences in the obtained TS.

A trigonal geometry is observed for the [Au(IMes)Cl] and DMSO TS, with Au-S and Au-Cl distances of 2.53 Å and 2.55 Å, respectively. The DMSO molecule approaches the Au(I) center at an angle of 83.5°. Similarly, the reaction with Cys^- also occurs via a trigonal TS, with Au-S and Au-Cl bonds of 2.73 and 2.42 Å, forming a 94.0° angle. These results suggest an associative mechanism consistent with previous studies that showed that Au(I) tends to react through trigonal transition states in substitution reactions[26].

In contrast, any of the [Cu(IMes)Cl] substitution TS structures exhibit both *L* and Cl^- coordinated at the Cu(I) center simultaneously. The DMSO TS has the DMSO molecule coordinated with a Cu-S bond of 2.22 Å and a dissociated Cl^- with a Cu-Cl distance of 3.80 Å, forming an S-Cu-Cl angle of 77.6°. Another difference to the [Au(IMes)Cl] DMSO TS is that the C-Cu-S angle is considerably broader than the C-Au-S, indicating that the [Cu(IMes)Cl] DMSO reaction occurs via a TS where the DMSO approximation to the Cu(I) center leads to the Cl^- dissociation, while, in the [Au(IMes)Cl] counterpart this does not necessarily occur since Au(I) has a larger ionic radius than Cu(I) and can accommodate simultaneous coordination easier.

Similarly, the TS of the [Cu(IMes)Cl] Cys^- reaction has a Cu-S distance of 3.27 Å before formal bond formation while preserving the Cu-Cl bond with 2.18 Å and Cl-Cu-S angle of 95.9°,

indicating the mechanism has a dissociative component. Even at a Cu-Cys distance of 3.27 Å, the weakening of the Cu-Cl bond can be seen by the increase in length.

The differences in the TS structures can explain the higher activation energy (ΔG (R→TS) = 13.69 kJ/mol) of [Au(IMes)Cl] than the [Cu(IMes)Cl]. The Au(I) compound assumes a trigonal TS suggesting an associative mechanism, which implies an increased stereo-electronic strain compared to the [Cu(IMes)Cl]. While the impact of this strain is lower for the DMSO reaction (both reactions have close activation energy), even if the TS structures suggest different mechanisms. The [Cu(IMes)Cl] Cys^- substitution has lower activation energy, whereas the reaction with [Au(IMes)Cl] is thermodynamically more favorable. While the ΔG (R→PA) of the former is 15.32 kJ/mol, for [Au(IMes)Cl] is -13.97 kJ/mol. At the production formation step, the ΔG (R→P) for [Au(IMes)Cl] is -19.06 kJ/mol more negative than for [Cu(IMes)Cl]. This illustrates the affinity of Au(I) centers for soft thiolate groups, as the Cys-, and the relative stability of the formed product, [Au(IMes)Cys].

There are also some notable dissimilarities in the ligand scrambling TS structures. In the case of [Cu(IMes)Cl], one of the IMes molecules binds to two Cu(I) centers, which effectively brings the metals closer together to form a metal-metal bond with 2.43 Å. The Cu-C bonds from the same IMes molecule are unequally lengthened, a shorter one with 2.00 Å, and a longer one with 2.31 Å, forming a trigonal structure with one of its angles, C-Cu-Cu, of 62.1°. Another IMes molecule is coordinated with the other Cu(I) center forming a 1.98 Å bond, which is close to the other 2.00 Å Cu-C bond in this TS. Besides that, in this TS, both Cl^- appear coordinated to one of the Cu(I) centers, which resembles the $[CuCl_2]^-$ molecule formed at the end of the reaction. This TS suggested a concerted associative mechanism as previously reported for Ag(I)NHC scrambling reactions[27]. In contrast, the [Au(IMes)Cl] ligand scrambling TS depicts a molecule of

[Au(IMes)Cl] being attacked by a second one. The first molecule has its Au(I) center presenting a trigonal geometry and Au-Cl, Au-C bonds at values 2.28 Å, 1.97 Å, respectively, and C-Au-Cl angle at 173.7° which are close to the ones of isolated [Au(IMes)Cl], 2.30 Å, 1.98 Å and 178.7°. The second molecule has its Cl^- dissociated, forming an aurophilic interaction with the other Au(I), with 2.77 Å.

Goetzfried et al. proposed a mechanism for the ligand scrambling reaction of a [Au(NHC)Br] complex, using 3-ethyl-4-(4-methoxyphenyl)-5-(2-methoxypyridin-5-yl)-1-propylimida-zol-2-ylidene) as the NHC ligand[26]. Several transition states and intermediate structures were identified, mostly exhibiting aurophilic interactions. The TS structures revealed that the highest energy barrier observed was 85.3 kJ/mol (20.4 kcal/mol), significantly lower than that of [Au(IMes)Cl] at 196.15 kJ/mol (46.84 kcal/mol). The ligand studied by Goetzfried et al. featured smaller substituents at the nitrogen position of the NHC than IMes. Consequently, considering the influence of the halide anion on the TS structures is limited, this energy difference indicates that [Au(IMes)Cl] is more inert than [Au(NHC)Br], supporting the hypothesis that steric hindrance imposed by the NHC ligand reduces ligand scrambling reactions[8].

There are reports in the literature of aurophilic interactions in TS of Au(I)-NHC ligand scrambling reactions. Even though metallophilic interactions are much more common for heavy metals, such as Au and Hg; there are also reports on cuprophilic interactions, like those observed in the TS depicted in Figure 2f[15].

Figure 3c shows that the ligand scrambling reaction is more favorable kinetically and thermodynamically for [Cu(IMes)Cl] than for [Au(IMes)Cl]. There is a significant difference in the activation barrier of the two reactions, with the [Cu(IMes)Cl] being 68.06 kJ/mol lower than the Au(I) counterpart. An explanation for such a difference lies in the relative stability of the TS

structures of each reaction. The Cu(I) seems to be more stable due to the binding of the two Cu(I) centers supported by one of the IMes molecules. Furthermore, these data support experimental observations obtained by NMR, in which the speciation ratio (i.e., the formation of the $[Cu(IMes)_2]^+$ and $[Au(IMes)_2]^+$ species) occurs to a greater extent and faster for the Cu(I) complex than for the Au(I) complex.

CONCLUSIONS

In this study, we investigated the reactions of [Au(IMes)Cl] and [Cu(IMes)Cl] organometallic complexes, focusing on their interactions with solvents and amino acids, such as dimethylsulfoxide (DMSO) and cysteine, and in the ligand scrambling reaction. The obtained results provide valuable insights into the mechanisms and energetics of these reactions, shedding light on the potential parallel reactions these drug-candidate compounds may undergo during *in vitro* tests.

In DMSO solutions, the three ligand exchange reactions compete. Notably, the exchange with cysteine displayed lower energy barriers and was thermodynamically favorable for both complexes, while the substitution by DMSO and ligand scrambling reactions were energetically unfavorable. Although the reaction with DMSO exhibited faster kinetics, the formation of the homoleptic $[M(IMes)_2]^+$ species was more predominant than the formation of $[M(IMes)(DMSO)]^+$ at equilibrium. Consequently, when evaluating the activity of [M(IMes)Cl] in *in vitro* tests, the speciation product, consisting of $[M(IMes)_2]^+$ molecules, becomes more relevant than $[M(IMes)DMSO]^+$.

However, both substitutions were less energetically favorable compared to the reaction with Cys, indicating the complexes' affinity for cysteine residues, confirming the potential targeting of

activated Cys residues in the active sites of enzymes such as thioredoxin, trypanothione, and glutathione reductases and cysteine proteases.

Previous studies mainly focused on the ligand scrambling reaction of [Au(NHC)X] complexes. This work explores and discusses ligand substitution reactions with biologically relevant nucleophiles, and our findings underscore the significance of incorporating simple ligand substitution reactions into these investigations. Notably, the exchange with Cys^- demonstrates both faster kinetics and greater thermodynamic favorability compared to the speciation into $[M(IMes)_2]^+$, emphasizing the importance of not disregarding simple ligand substitution in this line of inquiry.

By studying Au(I) and Cu(I) complexes, inertness and stability comparison was possible. Since the ligand scrambling reaction is more favorable for [Cu(IMes)Cl] than [Au(IMes)Cl], the formation of $[M(IMes)_2]^+$ for the Cu(I) complex becomes more relevant than for the Au(I) complex, making it a point of interest.

Additionally, it is important to acknowledge that the computational conditions employed may not fully capture the complex interactions and influences present in biological environments, such as energetic coupling with other steps, which could lead to overall reactions with different energy variations and the presence of solvent molecules, which could interact differently with the structures and alter their energies. Furthermore, a single molecule model representing the interaction with cysteine residues may deviate from experimental results, as these residues are typically part of larger macromolecules with additional components that can influence the outcomes.

More specific methods can address these considerations in future studies. However, despite the limitations of our current approach, the results obtained agree with experimental observations.

These findings can serve as a framework for interpreting *in vitro* experiments of the investigated drug candidates and guide the research and design of drug candidates.

ACKNOWLEDGMENT

This study was supported by São Paulo Research Foundation (FAPESP) Grants # 2022/02618-0 and #2020/11727-2, #2013/07296-2, #2016/23891-6, #2017/26105-4 and Brazilian Council for Scientific and Technological Development (CNPq) Grant # 404668/2021-6. We thank the CENAPAD Project #168 for computational resources and support.

ASSOCIATED CONTENT

Electronic Supporting Information contains additional figures and data.

REFERENCE

(1) Benedek, T. G. The History of Gold Therapy for Tuberculosis. *Journal of the History of Medicine and Allied Sciences* **2004**, *59* (1), 50–89. https://doi.org/10.1093/JHMAS/JRG042.

(2) Kean, W. F.; Forestier, F.; Kassam, Y.; Buchanan, W. W.; Rooney, P. J. The History of Gold Therapy in Rheumatoid Disease. *Seminars in Arthritis and Rheumatims* **1985**, *14* (3), 180–186. https://doi.org/10.1016/0049-0172(85)90037-X.

(3) Bulman, C. A.; Bidlow, C. M.; Lustigman, S.; Cho-Ngwa, F.; Williams, D.; Rascón, A. A.; Tricoche, N.; Samje, M.; Bell, A.; Suzuki, B.; Lim, K. C.; Supakorndej, N.; Supakorndej, P.; Wolfe, A. R.; Knudsen, G. M.; Chen, S.; Wilson, C.; Ang, K. H.; Arkin, M.; Gut, J.; Franklin, C.; Marcellino, C.; McKerrow, J. H.; Debnath, A.; Sakanari, J. A. Repurposing Auranofin as a Lead Candidate for Treatment of Lymphatic Filariasis and Onchocerciasis. *PLOS Neglected Tropical Diseases* **2015**, *9* (2), e0003534. https://doi.org/10.1371/JOURNAL.PNTD.0003534.

(4) Dominelli, B.; Ao, J. ~; Correia, D. G.; Kühn, F. E. Medicinal Applications of Gold(I/III)-Based Complexes Bearing N-Heterocyclic Carbene and Phosphine Ligands. *Journal of Organometallic Chemistry* **2018**, *866*, 153-164. https://doi.org/10.1016/j.jorganchem.2018.04.023.

(5) Rosa, L. B.; Aires, R. L.; Oliveira, L. S.; Fontes, J. V; Miguel, D. C.; Abbehausen, C. A "Golden Age" for the Discovery of New Antileishmanial Agents: Current Status of Leishmanicidal Gold Complexes and Prospective Targets beyond the Trypanothione System. *ChemMedChem* **2021**, *16* (11), 1681-1832. https://doi.org/10.1002/cmdc.202100022.

(6) Aires, R. L.; Santos, I. A.; Fontes, J. V.; Bergamini, F. R. G.; Jardim, A. C. G.; Abbehausen, C. Triphenylphosphine Gold(I) Derivatives Promote Antiviral Effects against the Chikungunya Virus. *Metallomics* **2022**, *14* (8). https://doi.org/10.1093/MTOMCS/MFAC056.

(7) Rothan, H. A.; Stone, S.; Natekar, J.; Kumari, P.; Arora, K.; Kumar, M. The FDA-Approved Gold Drug Auranofin Inhibits Novel Coronavirus (SARS-COV-2) Replication and Attenuates Inflammation in Human Cells. *Virology* **2020**, *547*, 7-11. https://doi.org/10.1016/j.virol.2020.05.002.

(8) Fontes, J. V.; Santos, I. A.; Rosa, L. B.; Lima, R. L. A.; Jardim, A. C. G.; Miguel, D. C.; Abbehausen, C. Antileishmanial and Anti-Chikungunya Activity of Cu(I)-N-Heterocyclic Carbenes. *ChemistrySelect* **2022**, *7* (31). e202201560. https://doi.org/10.1002/SLCT.202201560.

(9) Ge, E. J.; Bush, A. I.; Casini, A.; Cobine, P. A.; Cross, J. R.; DeNicola, G. M.; Ping Dou, Q.; Franz, K. J.; Gohil, V. M.; Gupta, S.; Kaler, S. G.; Lutsenko, S.; Mittal, V.; Petris, M. J.; Polishchuk, R.; Ralle, M.; Schilsky, M. L.; Tonks, N. K.; Vahdat, L. T.; Aelst, L.; Xi, D.; Yuan, P.; Brady, D. C.; Chang, C. J. Connecting Copper and Cancer: From Transition Metal Signalling to Metalloplasia. *Nature Reviews Cancer* **2022**, *22,* 102-113. https://doi.org/10.1038/s41568-021-00417-2.

(10) Jiang, Y.; Huo, Z.; Qi, X.; Zuo, T.; Wu, Z. Copper-Induced Tumor Cell Death Mechanisms and Antitumor Theragnostic Applications of Copper Complexes. *Nanomedicine (Lond)* **2022**, *17* (5), 303–324. https://doi.org/10.2217/NNM-2021-0374.

(11) da Silva, D. A.; De Luca, A.; Squitti, R.; Rongioletti, M.; Rossi, L.; Machado, C. M. L.; Cerchiaro, G. Copper in Tumors and the Use of Copper-Based Compounds in Cancer Treatment. *Journal of Inorganic Biochemistry*. **2022**, *226*. https://doi.org/10.1016/J.JINORGBIO.2021.111634.

(12) Herrera, R. P.; Gimeno, M. C. Main Avenues in Gold Coordination Chemistry. *Chemical Reviews* **2021**, *121* (14), 8311–8363. https://doi.org/10.1021/acs.chemrev.0c00930

(13) Troyano, J.; Zapata, E.; Perles, J.; Amo-Ochoa, P.; Fernández-Moreira, V.; Martínez, J. I.; Zamora, F.; Delgado, S. Multifunctional Copper(I) Coordination Polymers with Aromatic Mono- and Ditopic Thioamides. *Inorganic Chemistry* **2019**, *58* (5), 3290–3301. https://doi.org/10.1021/acs.inorgchem.8b03364

(14) Almotawa, R. M.; Aljomaih, G.; Trujillo, D. V.; Nesterov, V. N.; Rawashdeh-Omary, M. A. New Coordination Polymers of Copper(I) and Silver(I) with Pyrazine and Piperazine: A Step Toward "Green" Chemistry and Optoelectronic Applications. *Inorganic Chemistry* **2018**, *57* (16), 9962–9976. https://doi.org/10.1021/acs.inorgchem.8b01131

(15) Harisomayajula, N. V. S.; Makovetskyi, S.; Tsai, Y. C. Cuprophilic Interactions in and between Molecular Entities. *Chemistry* **2019**, *25* (38), 8936–8954. https://doi.org/10.1002/CHEM.201900332.

(16) Koskinen, L.; Jä, S.; Kalenius, E.; Hirva, P.; Haukka, M. Role of C–H···Au and Aurophilic Supramolecular Interactions in Gold–Thione Complexes. *Crystal Growth & Design* **2014**. https://doi.org/10.1021/cg500102c.

(17) Huynh, H. V. Group 11 Metal-NHC Complexes. *The Organometallic Chemistry of N-heterocyclic Carbenes* **2017**, 171–219. https://doi.org/10.1002/9781118698785.CH6.

(18) Ott, I. Chapter Five – Medicinal Chemistry of Metal N-Heterocyclic Carbene (NHC) Complexes. *Inorganic and Organometallic Transition Metal Complexes with Biological Molecules and Living Cells* **2017**, 147-179. https://doi.org/10.1016/B978-0-12-803814-7.00005-8.

(19) Lazreg, F.; Cazin, C. S. J. Medical Applications of NHC–Gold and –Copper Complexes. *N-Heterocyclic Carbenes: Effective Tools for Organometallic Synthesis* **2014**, *9783527334902*, 173–198. https://doi.org/10.1002/9783527671229.CH07.

(20) Rosa, L. B.; Galuppo, C.; Lima, R. L. A.; Fontes, J. V.; Siqueira, F. S.; Júdice, W. A. S.; Abbehausen, C.; Miguel, D. C. Antileishmanial Activity and Insights into the Mechanisms of Action of Symmetric Au(I) Benzyl and Aryl-N-Heterocyclic Carbenes. *Journal of Inorganic Biochemistry* **2022**, *229*. https://doi.org/10.1016/J.JINORGBIO.2022.111726.

(21) Pia Rigobello, M.; Messori, L.; Marcon, G.; Agostina Cinellu, M.; Bragadin, M.; Folda, A.; Scutari, G.; Bindoli, A. Gold Complexes Inhibit Mitochondrial Thioredoxin Reductase: Consequences on Mitochondrial Functions. *Journal of Inorganic Biochemistry* **2004**, *98* (10 SPEC. ISS.), 1634–1641. https://doi.org/10.1016/j.jinorgbio.2004.04.020.

(22) Ilari, A.; Baiocco, P.; Messori, L.; Fiorillo, A.; Boffi, A.; Gramiccia, M.; Di Muccio, T.; Colotti, G. A Gold-Containing Drug against Parasitic Polyamine Metabolism: The X-Ray Structure of Trypanothione Reductase from Leishmania Infantum in Complex with Auranofin Reveals a Dual Mechanism of Enzyme Inhibition. *Amino Acids* **2012**, *42* (2–3), 803–811. https://doi.org/10.1007/s00726-011-0997-9.

(23) Angelucci, F.; Sayed, A. A.; Williams, D. L.; Boumis, G.; Brunori, M.; Dimastrogiovanni, D.; Miele, A. E.; Pauly, F.; Bellelli, A. Inhibition of Schistosoma Mansoni Thioredoxin-Glutathione Reductase by Auranofin: Structural and Kinetic Aspects. *Journal of Biological Chemistry* **2009**, *284* (42), 28977–28985. https://doi.org/10.1074/JBC.M109.020701.

(24) Mirabelli, C. K.; Johnson, R. K.; Sung, C.; Faucette, L.; Muirhead, K.; Crooke, S. T. Evaluation of the in Vivo Antitumor Activity and in Vitro Cytotoxic Properties of Auranofin, a Coordinated Gold Compound, in Murine Tumor Models. *Cancer Research* **1985**, *45*, 32–39. PMID: 3917372.

(25) Hormann-Arendt, A. L.; Shaw, C. F. Ligand-Scrambling Reactions of Cyano(Trialkyl/Triarylphosphine)Gold(I) Complexes: Examination of Factors Influencing the Equilibrium Constant. *Inorganic Chemistry* **1990**, *29* (23), 4683–4687. https://doi.org/10.1021/ic00348a019.

(26) Goetzfried, S. K.; Gallati, C. M.; Cziferszky, M.; Talmazan, R. A.; Wurst, K.; Liedl, K. R.; Podewitz, M.; Gust, R. N-Heterocyclic Carbene Gold(I) Complexes: Mechanism of the

Ligand Scrambling Reaction and Their Oxidation to Gold(III) in Aqueous Solutions. *Inorganic Chemistry* **2020**, *59* (20), 15312–15323. https://doi.org/10.1021/acs.inorgchem.0c02298.

(27) Wang, H. M. J.; Lin, I. J. B. Facile Synthesis of Silver(I)-Carbene Complexes. Useful Carbene Transfer Agents. *Organometallics* **1998**, *17* (5), 972–975. https://doi.org/10.1021/om9709704.

(28) Dos Santos, H. F.; Vieira, M. A.; Sánchez Delgado, G. Y.; Paschoal, D. Ligand Exchange Reaction of Au(I) R-N-Heterocyclic Carbene Complexes with Cysteine. *Journal of Physical Chemistry A* **2016**, *120* (14), 2250–2259. https://doi.org/10.1021/acs.jpca.6b01052

(29) Tolbatov, I.; Coletti, C.; Marrone, A.; Re, N. Insight into the Substitution Mechanism of Antitumor Au(I) N-Heterocyclic Carbene Complexes by Cysteine and Selenocysteine. *Inorganic Chemistry* **2020**, *59* (5), 3312–3320. https://doi.org/10.1021/acs.inorgchem.0c00106.

(30) Tolbatov, I.; Marzo, T.; Coletti, C.; La Mendola, D.; Storchi, L.; Re, N.; Marrone, A. Reactivity of Antitumor Coinage Metal-Based N-Heterocyclic Carbene Complexes with Cysteine and Selenocysteine Protein Sites. *Journal of Inorganic Biochemistry* **2021**, *223*. https://doi.org/10.1016/J.JINORGBIO.2021.111533.

(31) Su, H. L.; Pérez, L. M.; Lee, S. J.; Reibenspies, J. H.; Bazzi, H. S.; Bergbreiter, D. E. Studies of Ligand Exchange in N-Heterocyclic Carbene Silver(I) Complexes. *Organometallics* **2012**, *31* (10), 4063–4071. https://doi.org/10.1021/om300340w

(32) Neese, F.; Wiley, J. The ORCA Program System. *Wiley Interdisciplinary Reviews: Computational Molecular Science* **2012**, *2* (1), 73–78. https://doi.org/10.1002/WCMS.81.

(33) Neese, F.; Wennmohs, F.; Becker, U.; Riplinger, C. The ORCA Quantum Chemistry Program Package. *Journal of Chemical Physics* **2020**, *152* (22), 224108. https://doi.org/10.1063/5.0004608/1061982.

(34) Ernzerhof, M.; Scuseria, G. E. Assessment of the Perdew-Burke-Ernzerhof Exchange-Correlation Functional. *Journal of Chemical Physics* **1999**, *110* (11), 5029–5036. https://doi.org/10.1063/1.478401.

(35) Weigend, F.; Ahlrichs, R. Balanced Basis Sets of Split Valence, Triple Zeta Valence and Quadruple Zeta Valence Quality for H to Rn: Design and Assessment of Accuracy. *Physical Chemistry Chemical Physics* **2005**, *7* (18), 3297–3305. https://doi.org/10.1039/b508541a.

(36) Kossmann, S.; Neese, F. Efficient Structure Optimization with Second-Order Many-Body Perturbation Theory: The RIJCOSX-MP2 Method. *Journal of Chemical Theory and Computation* **2010**, *6* (8), 2325-2338. https://doi.org/10.1021/ct100199k.

(37) Tomasi, J.; Mennucci, B.; Cammi, R. Quantum Mechanical Continuum Solvation Models. *Chemical Reviews* **2005**, *105* (8), 2999–3093. https://doi.org/10.1021/cr9904009.

(38) Debefve, L. M.; Pollock, C. J. Systematic Assessment of DFT Methods for Geometry Optimization of Mononuclear Platinum-Containing Complexes. *Physical Chemistry Chemical Physics* **2021**, *23* (43), 24780–24788. https://doi.org/10.1039/D1CP01851E.

(39) Fukui, K. Role of Frontier Orbitals in Chemical Reactions. *Science* **1982**, *218* (4574), 747–754. https://doi.org/10.1126/science.218.4574.747.

(40) Makedonas, C.; Mitsopoulou, C. A. An Investigation of the Reactivity of [(Diimine)(Dithiolato)M] Complexes Using the Fukui Functions Concept. *European Journal of Inorganic Chemistry* **2006**, *2006* (3), 590–598. https://doi.org/10.1002/EJIC.200500664.

(41) Bannwarth, C.; Ehlert, S.; Grimme, S. GFN2-XTB - An Accurate and Broadly Parametrized Self-Consistent Tight-Binding Quantum Chemical Method with Multipole Electrostatics and Density-Dependent Dispersion Contributions. *Journal of Chemical Theory and Computation* **2019**, *15* (3), 1652–1671. https://doi.org/10.1021/acs.jctc.8b01176.

(42) De Frémont, P.; Scott, N. M.; Stevens, E. D.; Nolan, S. P. Synthesis and Structural Characterization of N-Heterocyclic Carbene Gold(I) Complexes. *Organometallics* **2005**, *24* (10), 2411-2418. https://doi.org/10.1021/om050111c.

(43) Díez-González, S.; Escudero-Adán, E. C.; Benet-Buchholz, J.; Stevens, E. D.; Slawin, A. M. Z.; Nolan, S. P. [(NHC)CuX] Complexes: Synthesis, Characterization and Catalytic Activities in Reduction Reactions and Click Chemistry. On the Advantage of Using Well-Defined Catalytic Systems. *Dalton Transactions* **2010**, *39* (32), 7595–7606. https://doi.org/10.1039/C0DT00218F.

(44) Bhabak, K. P.; Bhuyan, B. J.; Mugesh, G. Bioinorganic and Medicinal Chemistry: Aspects of Gold(i)-Protein Complexes. *Dalton Transactions* **2011**, *40* (10), 2099–2111. https://doi.org/10.1039/C0DT01057J.

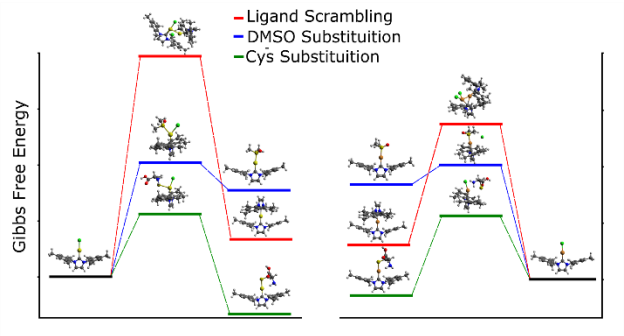

(8.250 x 4.450 cm)